Knife-Edge Technique Using Raman Spectrometers to Determine the Effective Laser Spot Size on Powders: Implications for Planetary Exploration

Lucas Demaret[1,2], Ian B. Hutchinson[3], Hannah N. Lerman[3], Melissa McHugh[3], Gauthier Eppe[1] and Cedric Malherbe[1,2,3]

1 Mass Spectrometry Laboratory, MolSys Research Unit, University of Liège, Liège, Belgium
2 Early Life Traces & Evolution-Astrobiology, UR Astrobiology, University of Liège, Liège, Belgium
3 Department of Physics and Astronomy, University of Leicester, Leicester, UK

Corresponding Author:
Mass Spectrometry Laboratory, University of Liège, MolSys Research Unit,
Allee du 6 Aout, 11 (B6c), Liege 4000, Belgium; Early Life Traces and
Evolution Laboratory-Astrobiology, University of Liège, Liege 4000, Belgium; Department of Physics and Astronomy, University of Leicester, Leicester LE1 7RH, UK. Email: C.Malherbe@uliege.be

Abstract
Raman spectroscopy is an analytical technique of choice for Earth and planetary sciences, which was recently selected as part of robotic exploration missions on Mars. Indeed, several miniaturized Raman spectrometers have been included into the scientific payload of rovers for the remote surface exploration of Mars: SuperCam and Scanning Habitable Environments with Raman and Luminescence for Organics and Chemicals (SHERLOC) for the NASA Mars 2020 mission and the Raman laser spectrometer (RLS) for the European Space Agency's (ESA) ExoMars mission. In preparation for these missions, a number of Mars analogue biogeological samples retrieved on Earth are extensively interrogated using Raman spectrometers, including flight prototype instruments but not only. Some studies also used flight representative portable instruments, as well as benchtop instruments. Commonly, authors reported the excitation laser wavelength and its power but often omitted the laser spot size on the sample which is a key factor for comparing several studies in term of spectrometer capabilities. In this study, we reported an easy, fast and universal experimental approach for determining the effective laser spot size, defined as the diameter of the sample section which is effectively probed by the Raman spectrometer during the analyses. Here, we characterized the effective laser spot size for a benchtop micro-Raman system and two different portable spectrometers, using a standard silicon wafer and gypsum powders with various average grain sizes. The dependence of the laser spot size with the grain size of the samples is discussed with regards to qualitative and quantitative analyses of solid dispersions in the scope of remote planetary missions.

Keywords
Raman, spot size, laser, grain size, intensity, knife-edge, planetary exploration

Introduction

Miniaturized Raman instruments are constantly being developed for many different applications in the fields of geology, art, archaeology, forensic sciences, biomedical sciences and space sciences.[1–4] Indeed, Raman spectroscopy offers many reasons to be considered for analytical investigations: it provides molecular information about a sample, typical recording times are in the range between 1 s to a few minutes, analysis can be performed through a transparent container or protective film, often in a non-destructive way. Raman spectroscopy can even be performed using a remote illumination system linked to the spectrometer via optical fibers. In addition, miniaturized Raman spectrometers have the ability to interrogate inorganic, organic as well as biological materials. Certainly, it is because of these advantages that Raman spectroscopy instruments have been proposed for a number of recent planetary missions, especially on Mars. The NASA Mars

2020 mission includes two miniaturized Raman instruments (one using a 532 nm excitation source and one using a 249 nm excitation source) to study the surface of Mars. The ESA's ExoMars mission also includes a Raman laser spectrometer (RLS) as part of the Rosalind Franklin payload suite of analytical instruments to conduct analyses of the planetary surface and subsurface.[5] The scientific aims of the Raman instruments on board of both missions are to investigate the planet's habitability by studying the mineralogy of the surface and subsurface and to search for organic compounds that could represent evidence for past or surviving forms of life.[6,7] Despite clear advantages, the Raman spectroscopy technique also suffers from some specific limitations, mainly because Raman scattering is a relatively weak physical effect that requires high-intensity, monochromatic light sources (e.g., lasers). Another issue is that the Raman spectra can be affected by various interfering signals, either coming from the sample itself (e.g., luminescence) or from the outer environment (e.g., ambient light or cosmic rays). The quality of the Raman spectra obtained is therefore dependent on both the specific nature of the sample under investigation and the design and operation of the instrument.

When designing, optimizing and commissioning particular instrument concepts for remote exploration missions (either in space or in area on Earth inaccessible to human), comprehensive testing is critical and are often performed using either natural or synthesized samples similar to those that will be ultimately studied with the specific instrument. This is especially true for space applications where it will be difficult (or impossible) to modify the design/operation of the instrument after launch. For example, in preparation for the exploration missions of Mars, analogue samples (samples found in extreme terrestrial environments that replicate the severe conditions expected on Mars) are thoroughly investigated using flight representative Raman spectrometers. Typical analog samples for those missions include (but are not restricted to) meteorites, stromatolite, regolith, halite, hydrated sulfates and iron (oxy) hydroxides, desert varnish, basalt and volcanic rocks, shale and mudstone, sandstone, and fossilized sedimentary rocks, often containing epilithic or endolithic colonisations.[8–21] These studies have demonstrated that Raman instruments are indeed excellent for the detection of various geomarkers and biomarkers, in particular those associated with microorganisms able to survive in extreme habitats. However, a direct comparison of the studies (in terms of spectral performance) is not straightforward since various excitation wavelengths (from ultraviolet to near infrared) were used, with a range of various Raman instrument configurations and operating parameters utilized (i.e., laser spot sizes, or footprint, laser power levels and sampling techniques/exposure times).

The Raman instruments used for planetary studies and astrobiology can be classified into two categories of instrumentation: benchtop and portable. Benchtop Raman instruments are designed for laboratory use and are therefore not intended to be moved from one site to another. Their developments are mainly governed by spectroscopic efficiency such as high spectral resolution, high signal to noise ratio and fine spatial resolution (most benchtop Raman instruments are actually coupled to microscopes enabling to achieve micrometric illumination of the sample). Consequently, these instruments are often voluminous and relatively heavy. Contrarily, portable Raman spectrometers (including handheld instruments) are designed to be readily transported from one location to another and enable field experiments.[2,4] These portable spectrometers are conceived to be light, so that they can be carried by a single person or a robot, and stable. They do not require any optical adjustment prior to operation (the excitation laser is incorporated inside the instrument, and each optical element is firmly fixed in place). However, the weight and size limitations influence the overall instrument performance, especially in term of spectral and spatial resolution (typically around 10 cm^{-1} and ranging between 50 and 100 µm, respectively). As discussed by Vandenabeele et al.,[22] the limit of detection will be dependent upon experimental factors dictated by the design of the Raman instrument (including the laser power on the sample, the sample illumination optics, the observation geometry and the detector sensitivity) altogether with sample factors (sample composition, homogeneity, and the nature of the geological matrix, potentially fluorescent). Among other parameters, the laser spot size, defined as the laser's footprint on the sample in the instrument's focal plane, which sets the lower limit of spatial resolution, significantly affects the signal intensity and analytical performance, yet its impact is often overlooked. Indeed, the Raman intensity is directly proportional to the laser power density (also known as the irradiance) received by the sample.[23] Because the sample illumination systems are different for micro-benchtop (often operating with microscope objectives) and portable (operating with focusing lenses) instruments, the laser footprint is expected to be quite different (actually larger with portable instrument compared to micro-benchtop instrument), so is the Raman intensity observed with a given laser power. However, the laser spot size is not always known for a particular instrument, and most reported values are provided by the manufacturer of the instrument or theoretically predicted by Gaussian beam optics and formulae of focusing lenses.[23,24] Reporting the laser footprint as measured with specific instrument and optics would be a better approach.

Nowadays, two-dimensional (2D) cameras can directly image the laser footprint as delivered by a Raman spectrometer,[25] but not every laboratory is equipped with that equipment, and the estimated laser footprint is only representative of the laser footprint expected on a hard-flat surface of a homogeneous sample. In addition, many techniques

have been proposed in the literature to measure the diameter of a collimated laser beam. The general idea is to block partly and progressively the beam in a transect direction to the propagation axis. The laser beam diameter can be obtained from the slit scan technique,[26–28] or the pinhole technique,[27,29,30] when an aperture smaller than the spot size is used. The knife-edge technique (also referred to as scanning knife or edge-scan technique) is a fast and an inexpensive technique recognized as a standard method to determine the width of the laser beam.[31–34] The knife-edge technique consists in occluding progressively the beam with a sharp edge mask following a transect direction to the beam propagation and recording the integrated signal of the nonoccluded section of the beam. Since the intensity transect profile of most laser beams follow a 2D Gaussian profile G (x,y) the cross-section profile of the laser beam intensity in the focal plane is represented in Figure 1a, assuming a symmetric profile in the directions x and y (orthogonal to the propagation direction of the laser beam). The intensity of the laser beam is given by Eq. 1, where G_0 is the maximum of intensity at the coordinate (x_0, y_0), and ω is the radius at which the intensity drops to 1/e of its maximum value. That beam waist can be typically reported as the distance to the center for which the intensity is 1/e of its maximum (radius ω) or as the distance to the center for which the intensity is $1/e^2$ of its maximum (radius ω'). The two values only differ by a factor √2. These parameters can be used to determine the beam diameter (expressed as 2 ω or 2ω' and represented in Figure 1b). Other practical descriptions of the beam size can involve the full width at half-maximum (FWHM) or the full width at tenth of maximum (FWTM). The FWHM corresponds to the diameter for which the laser intensity drops to $G_0/2$, while the FWTM corresponds to the diameter for which the laser intensity drops to $G_0/10$.

$$G_{(x,y)} = G_0 \exp\left(-\frac{(x-x_0)^2 + (y-y_0)^2}{\omega^2}\right) \quad (1)$$

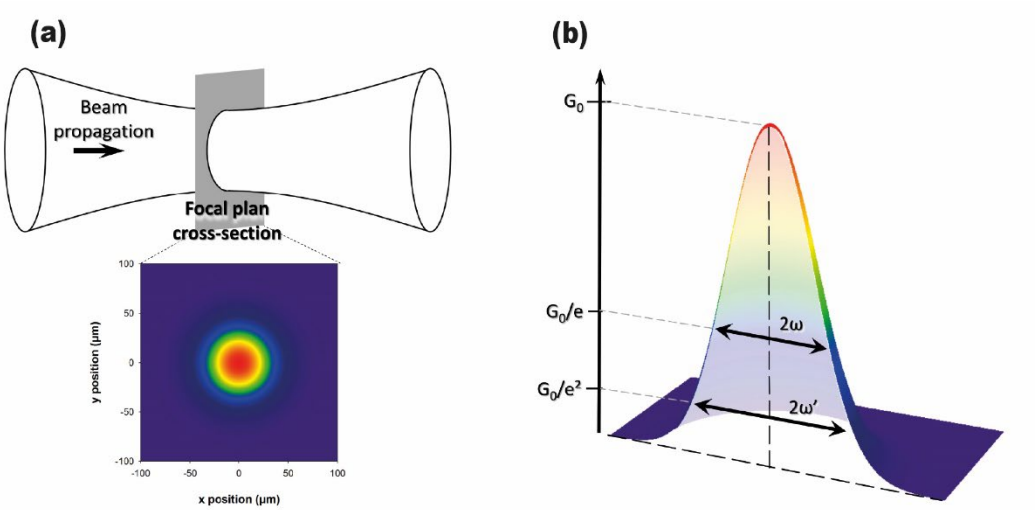

Figure 1: Intensity profile of a laser beam. (a) The focal plan cross-section showing a symmetric 2-dimensional Gaussian profile. (b) Beam width represented using two definitions: 2ω and 2ω'. The ω is the radius for which the intensity drops to 1/e from the maximum, while ω' is the radius for which the intensity drops to $1/e^2$ from the maximum.

The aforementioned techniques have proven very effective in estimating the laser footprint delivered by an optical instrument, including Raman instruments.[35,36] However, no simple experimental method has been proposed so far, and to the best of our knowledge, to evaluate the effective spot size considering the granulometry of a solid sample. Since powders are analyzed in many remote applications of Raman spectroscopy (robotic planetary exploration Raman spectrometers will, for instance, interrogate rock powders and soils), determining the effective laser spot size to apprehend its influence on both qualitative and quantitative applications is important.

In the frame of this work, the effective spot size is defined as the laser footprint on the sample from which the Raman signal is collected when performing a Raman analysis. We propose here to apply the knife-edge experimental technique on a flat silicon wafer to determine the effective laser spot size of various spectrometer, including two portable instruments operating at two different wavelengths (532 nm and 785 nm) and a benchtop micro-spectrometer operating at 532 nm with two different objective lenses. Then we applied the technique on powder samples to discuss how diffusing granular materials tend to increase the laser footprint, using the benchtop and the portable Raman system at 532 nm. In particular, different

grain size fractions of gypsum (10–50 µm, 50–100 µm, and 100–150 µm) were analyzed to determine how the effective spot size is influenced by the particle size. Finally, these dispersions were also employed to assess the influence of the grain size on the Raman intensities measured directly for either powders of pure gypsum or gypsum powders spiked with *L*-cysteine.

Experimental Materials and Methods

A single crystal (100) silicon wafer (0.8 mm in thickness) with a sharp edge was employed for estimating the laser footprint on a hard and flat sample by the knife-edge method. Polished silicon wafer with orientation (100) is considered a common reference material for Raman spectroscopy, and produces a sharp, well defined, and stable band at 520.5 cm^{-1}, corresponding to the triply degenerate first order optical phonons in the O_h point group of a diamond-type lattice.[37] Raman spectra were recorded across the sharp edge of the silicon wafer directly placed in the focal plane of the instrument.

Gypsum (dihydrated calcium sulfate) powders, with grains of increasing averaged size, were also employed to evaluate the effect of granulometry on the effective laser spot size as determined by the proposed experimental method. A crystalline gypsum specimen (hand-picked from Carresse, France) was crushed in an agate mortar and separated in three fractions with different granulometry using test sieves (mesh sizes: 50–100–150 µm). Gypsum powders with a particle size between 10–50, 50–100, and 100–150 µm were collected for Raman analyses. The powders were poured and flattened with a spatula into wells carved in a block of aluminium presenting no specific Raman signal. In this study, the strong and characteristic Raman band of gypsum at 1008 cm^{-1} ($SO^2{}_4{}^-$ stretching) was followed across the sharp edge formed at the interface of the gypsum powder and the edge of the aluminium sample holder.

Besides pure gypsum matrices, binary mixtures were also prepared by spiking *L*-cysteine (Merck 2838, purity 99%) at 10 wt% into each of the gypsum fraction (10–50, 50–100, and 100–150 µm). These types of binary mixtures have been studied previously for analytical spectroscopic developments in a context of planetary sciences missions.[38,39] *L*-Cysteine displays a strong and characteristic Raman band at 2545 cm^{-1} (S–H stretching).

Since the Raman signal intensity is proportional to the laser intensity, which follows a 2D Gaussian profile, the integrated signal $\tilde{G}$ (normalized to the full integrated signal) from a material (e.g., silicon or gypsum) as a function of the sharp edge position in the instrument focal plane is given by Eq. 2, in which Erf is the error function. With the knife-edge procedure proposed here, when the laser footprint does not overlap any part of the Raman active material in the focal plane, no Raman signal is recorded. This corresponds to the situation where the laser beam is entirely blocked in the classical knife-edge technique. When the laser overlaps entirely with the material surface, the Raman intensity is maximized, corresponding to the situation where the beam is not blocked in the classical knife-edge situation. Finally, when the laser spot overlaps partially with the sharp edge of the Raman active material, the Raman intensity is proportional to the laser intensity that reaches the sample. By analogy with the classical knife-edge method, this corresponds to the situation where the beam is partially blocked. During measurements, the laser was first focused on top of the sample surface in order to maximize the signal (when the footprint overlaps entirely with the sample), then the sample was moved progressively to scan the sample across the sharp edge (silicon wafer sharp edge or the aluminium powder interface depending on the sample). An example of the Raman signal evolution with a silicon sharp edge position is illustrated in Figure 2a. The error function in Eq. 2 is not an analytical function easy to use for fitting data, but de Araújo et al. demonstrated that it can be evaluated using the much simpler Eq. 3, where x' is given by Eq. 4, a_1 being equal to –1.597106847 and a_2 being equal to $-7.0924013 \times 10^{-2}$.[34] The beam waist ω, defined as the beam radius from the center to the distance where the intensity falls down 1/e of its maximum value, is often used to report the dimensions of a focused laser beam.[40,41]

$$\tilde{G}_{(x)} = \frac{1}{2}\left(1 + \mathrm{Erf}\left(\frac{x - x_0}{\omega}\right)\right) \tag{2}$$

$$\tilde{G}_{(x')} \cong \frac{1}{1 + \exp(a_1 x' + a_2 x'^3)} \tag{3}$$

$$x' = \frac{\sqrt{2}\,(x - x_0)}{\omega} \tag{4}$$

Intensity profiles were established by reporting the Raman intensity as a function of the sample sharp edge position (see example shown in Figure 2b). Afterwards, the profiles are fitted with Eq. 5 (directly derived from Eq. 3), where $I_{(x)}$ is the normalized Raman intensity of the material, I_0 is the normalized intensity when no Raman signal was detected (spectral background), I_{Max} is the maximum normalized Raman intensity of the material, a_1 equals –1.597106847, a_2 equals –7.0924013

× 10^{-2}, and ω is the radius at which the normalized Raman intensity drops to 1/e. I_0 takes into account that the noise is measured.

$$I_{(x)} = I_0 + \frac{I_{Max}}{1 + \exp\left(a_1\left(\frac{\sqrt{2}\,(x - x_0)}{\omega}\right) + a_2\left(\frac{\sqrt{2}\,(x - x_0)}{\omega}\right)^3\right)} \quad (5)$$

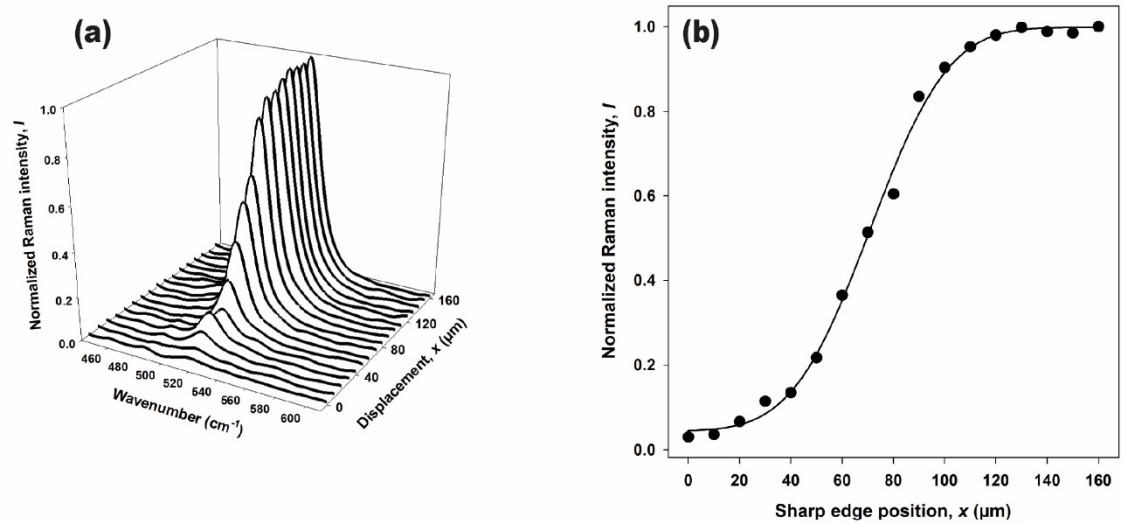

Figure 2: Evolution of the normalised Raman intensity for spectra recorded on top the silicon wafer as a function of the silicon sharp edge position. (a) Evolution of the Raman signal at 520.5 cm^{-1} in the spectra of silicon, recorded with the Raman Inspector spectrometer after baseline correction and normalisation of intensity. (b) Intensity profile of the silicon dataset fitted with the Eq. 5.

Raman Spectroscopy

In order to determine the effective laser footprint of a Raman instrument with the knife-edge method, a line scanning is applied perpendicularly to the sharp edge of the sample with spectra recorded at regular intervals. The Raman intensity profiles were constructed following the maximum height of the Raman band of interest (i.e., at 520.5 cm^{-1} for silicon, at 1008 cm^{-1} for gypsum, and at 2545 cm^{-1} for *L*-cysteine), on the baseline-corrected spectra (using a Savitzky–Golay polynomial fitting). All Raman profiles were performed in replicates (n > 3) per sample using three different Raman instruments: two commercial portable instruments manufactured by DeltaNu and a benchtop instrument manufactured by Horiba. The operating parameters of the portable spectrometers were similar to the flight operating modes of instruments designed for exploration missions on Mars.[42]

The first instrument was a handheld portable Raman Inspector (DeltaNu), operating a 785 nm excitation wavelength (able to irradiate the sample with a maximum power of 120 mW) and a thermoelectrically cooled charge-coupled device (CCD) detector. Data were obtained across the 200– 2000cm^{-1} wavenumber offset range with a spectral resolution of ~8 cm^{-1}. The second instrument was a Raman Advantage 532 spectrometer (DeltaNu), interfaced with a 532 nm excitation wavelength (Coherent DPSS 532 laser able to irradiate the sample with a maximum power of ~ 10 mW) and a thermoelectrically cooled CCD detector. Data were obtained across the 200–3400 cm^{-1} wavenumber offset range with a spectral resolution of ~10 cm^{-1}. A manual x,y translational stage (Thorlabs LX20/M) was used to move the sharp edge of the sample under each portable instrument for recording a Raman spectrum every 10 µm. Additionally, Raman mapping was performed on the powder samples to assess the influence of the grain size on the Raman signal intensity. A square grid pattern of 17 × 17 point-analysis, separated by a distance of 250 µm, was recorded on the sample surface to characterize the variation of the Raman intensity due to the surface roughness conferred by the stacking of grains in the solid dispersions. The third instrument was a LabRam 300 spectrometer (Horiba), interfaced with a 532.3 nm excitation wavelength (Cobolt Samba 532 DPSS laser, able to irradiate the sample with a maximum power of 150 mW) and a thermoelectrically cooled CCD detector Andor iDus DU401-BRDD. The spectrometer is coupled to an Olympus BX40 microscope equipped with an x,y computerized mobile stage (Märzhäuser Wetzlar SCANplus 75 × 50). Two objective lenses were used in this study, a 10 × objective, Edmund Microplan DIN 10 and

numerical aperture (NA) 0.25, with a focal distance of ~15 mm and an achromatic lens (NA: 0.18) with a focal distance of 50 mm. Raman spectra were recorded every 1 µm across the 200–2000 cm^{-1} wavenumber offset range with a spectral resolution of ~3 cm^{-1} (grating 1800 lines/mm) using the 10x objective, and every 10 µm, across the 100–4000 cm^{-1} wavenumber offset range with a resolution of ~10 cm^{-1} (grating 1200 lines/mm) using the achromatic lens.

Results and Discussion

Effective Laser Footprint on Silicon Wafer

The application of the knife-edge technique on a silicon wafer using the various spectrometers typically resulted in intensity profiles such as the profile presented in Figure 3a. The fitting of the data with Eq. 5 enabled to determine the radius of the beam when the intensity falls to 1/e of its maximum value, ω. In a few cases, the intensity measured at the sharp edge position was observed to be higher than the intensity measured on top of the silicon wafer, resulting in a profile similar to the profile in Figure 3b. This kind of profiles were observed when the edge at the location of the transect scan was actually not sharp enough. A microscopic pitch in the silicon wafer could be the origin of this deviation effect. However, data were still fitted successfully with Eq. 5 if outliers (hollow circles in Figure 3b) are discarded for the fitting.

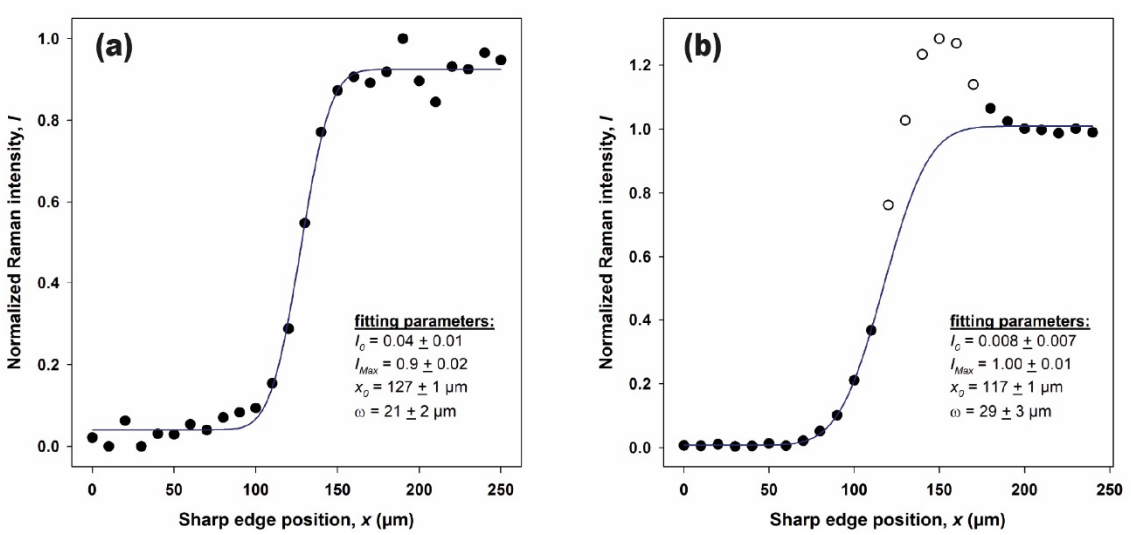

Figure 3: Fitting of intensity profiles for data obtained on silicon wafer, by Eq. 5. (a) Typical example of profile observed, along with the reported fitting parameters, for an experiment conducted with the Advantage 532 spectrometer. (b) Example of profile displaying sharp-edge distortions, along with the reported fitting parameters for an experiment conducted with the Inspector spectrometer. The fitting parameters are indicated with their associated standard error.

The values of the effective beam radius, ω, are summarized in Table I. An increase of ω, and thus of the beam diameter 2ω′ (2ω′ = 2√2ω) is clearly observed when replacing the 10× objective by the achromatic lens operated with the benchtop instrument, from a 2ω' value of 7.6 µm to37 µm, respectively. The portable (Advantage) and handheld (Inspector) spectrometers give a 2ω' value of 57 µm and 90 µm, respectively. Because these two instruments operate through long focal lenses, higher effective laser spot diameters were measured. Also, for the Raman Inspector instrument, the effective laser spot diameter reflects that the instrument is operating a 785 nm laser beam, which is initially larger than the 532 nm laser interfaced with the other instruments compared in this study.

Table 1. Summary of the laser beam parameter ω measured using 3 Raman instruments and a piece of silicon wafer with a sharp edge. ω is the radius from the centre of the laser spot at which the intensity drops to 1/e of the maximum intensity. The values for the individual experiments are reported with their standard errors and the mean ω are reported with their standard deviation.

Instruments (constructor)		Laser		Experiments on Si wafer (1)	(2)	(3)	Mean
Raman Inspector (DeltaNu)		785	ω (µm)	32 ± 3	34 ± 4	29 ± 3	32 ± 3
			2ω' (µm)	91 ± 8	96 ± 11	82 ± 8	90 ± 7
Advantage (DeltaNu)		532	ω (µm)	20 ± 2	21 ± 2	19 ± 3	20 ± 1
			2ω' (µm)	57 ± 6	59 ± 6	54 ± 8	57 ± 3
LabRam 300 (Horiba)	Lens	532	ω (µm)	13 ± 2	13 ± 2	13 ± 2	13 ± 0.1
			2ω' (µm)	37 ± 6	37 ± 6	37 ± 6	37 ± 0.2
	10x objective	532	ω (µm)	2.1 ± 0.2	2.6 ± 0.2	3.4 ± 0.4	2.7 ± 0.7
			2ω' (µm)	5.9 ± 0.6	7.4 ± 0.6	9.6 ± 1.1	7.6 ± 2

Effective Laser Footprint on Solid Powders as a Function of the Grain Size

The knife-edge technique was applied on gypsum powders constituted of grains with different sizes using the benchtop spectrometer (operating with the lens) and the Advantage 532 spectrometer. Typical Raman intensity profiles obtained for the powders are presented in Figure 4a. As opposed to the profiles obtained for silicon wafer, the Raman intensity in the plateau is not constant. In the plateau, the Raman intensity observed for the solid powders varies in response to the variation of the amount of gypsum in the depth of field due to the grains staked up in the aluminium support. Because that fluctuation can influence the fitting of the data, the fitting was performed on the mean profiles obtained from three different measurement series, as shown as the dotted line in Figure 4a. The normalized mean profiles were fitted with Eq. 5, as presented in Figure 4b to extract the ω values that are compiled in Table II.

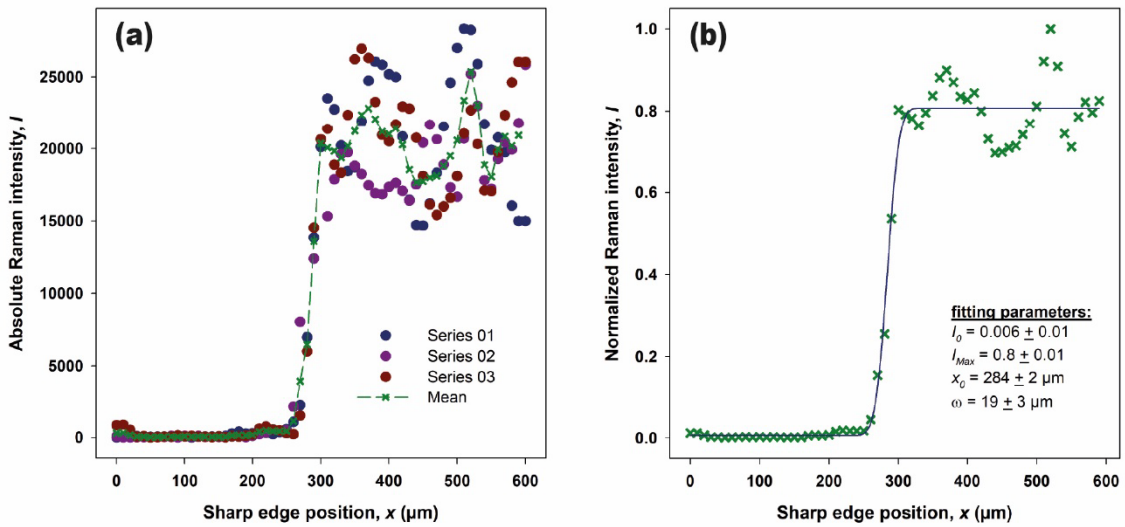

Figure 4: Intensity profiles for data obtained on gypsum dispersions. (a) Absolute intensities for 3 experiments of knife-edge on the gypsum powder fraction 100-150 µm using the benchtop spectrometer. The mean dataset from the 3 series is highlighted by a dotted line. (b) Fitting of intensity profile for the mean dataset, along with the reported fitting parameters. The fitting parameters are indicated with their associated standard error.

Compared to the previous situation where the effective laser spot size was determined on a flat isotropic silicon wafer, the values for ω determined on the flat surface of solid powders were statistically larger. Indeed, the effective beam diameter (2ω') on gypsum powders is almost twice the diameter observed on silicon wafer. For example, the laser footprint of the Advantage 532 spectrometer increased from ~ 57 µm (silicon) to >100 µm (gypsum powders), whereas the footprint from the benchtop system equipped with the lens increased from ~ 37 µm (silicon) to >50 µm (gypsum powders). Also, as indicated in

Table II, the effective beam diameter is influenced by the grain size. A decrease in 2ω' is observed when the grain size increases in the range between 10 and 150 µm. The most significant difference concerns the Advantage spectrometer, with an apparent spot of 122 µm for the finer grain size and a spot of 105 µm for the coarser grains size. The increase of the effective laser spot size observed for the gypsum powders compared to the effective laser spot size observed on silicon can be linked to both the nature and the physical state of the samples. Indeed, silicon is an isotropic absorbent solid material that does not allow the elastic laser scattering inside the solid material. In the other hand, the gypsum powders are constituted of transparent anisotropic grains that can elastically scatter the laser light inside the grainy solid material, leading to an apparent larger laser spot size from which the Raman signal is scattered (far-field molecular inelastic scattering). Multiple reflections occur at the grain boundary, which can also contribute to the enlargement of the apparent spot size observed with fine-grained gypsum powder compared to the coarse grains. These values of the effective laser spot size are consistent with previous general discussion reporting that the effective laser diameters are increased when analyzing powdered rocks and soils.[43]

Effect of the Grain Size on the Raman Intensity of Powders

The variation of the Raman intensity typically observed at 1008 cm^{-1} using the Advantage 532 spectrometer at the surface of the three fractions of gypsum powder is presented in Figure 5. Each dataset corresponds to 289 Raman spectra recorded on the top of the powder surface. The mean Raman intensity observed for each fraction seems to decrease as the average size of the grain increases: the mean Raman intensities for gypsum are 7500 ± 800, 6000 ± 1000, and 5000 ± 1000, respectively for the fractions with a grain size in the ranges 10–50 µm, 50–100 µm, and 100– 150 µm (Table III).

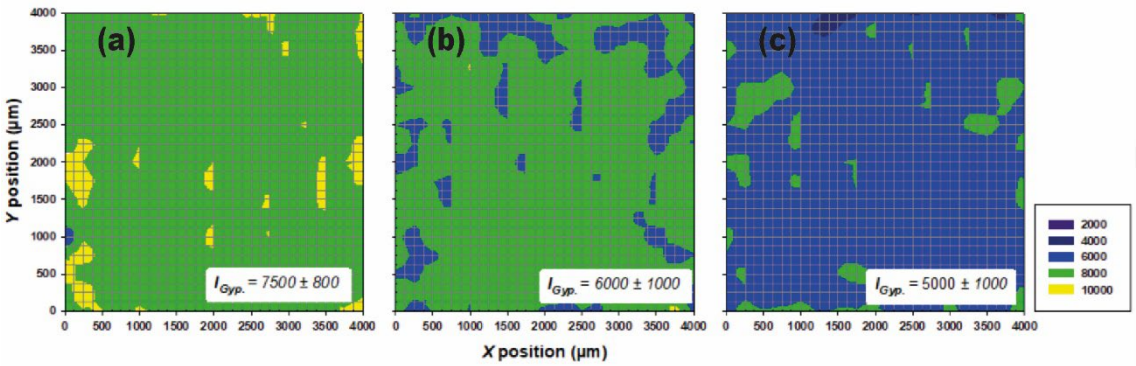

Figure 5: Raman mapping of gypsum dispersions having a grain size distribution of 10-50 µm (a), 50-100 µm (b) and 100-150 µm (c) using the Advantage 532 spectrometer. The mean intensity (I_{Gyp}) and the standard deviation for the values of gypsum (i=289) are reported for each mapping.

Table 3. Absolute Raman intensities for dispersions of gypsum blanks having different average grain sizes using the Advantage 532 spectrometer. Absolute intensities from gypsum (I_{Gyp}) are reported from mapping (i=289) in triplicates. All the values of intensity are reported with their standard deviation.

Grain Size		Raman intensity values ± SD obtained for 3 replicates on bulk gypsum powders			Mean ± SD
		(1)	(2)	(3)	
10 – 50 (µm)	I_{Gyp}	7500 ± 800	7200 ± 900	7200 ± 800	7300 ± 200
50 – 100 (µm)	I_{Gyp}	6500 ± 1000	6800 ± 1000	6800 ± 1000	6700 ± 200
100 – 150 (µm)	I_{Gyp}	5300 ± 1000	5500 ± 1000	5500 ± 1000	5400 ± 100

With a constant laser power delivered to the sample surface, the decrease of intensity seems to be correlated with the decrease of the apparent spot size (Table II). When the gypsum powders are spiked with *L*-cysteine at a concentration of 10 wt%, the average Raman signal observed for the *L*-cysteine also decreases as the gypsum matrix particle size increases (Table IV).

Table 4. Raman intensities evaluated from binary mixtures of gypsum spiked with *L*-cysteine at 10 wt% using the Advantage 532 spectrometer. Absolute intensities from gypsum (I_{Gyp}), and cysteine (I_{Cys}), are reported from mapping (i=289) in triplicates. All the values of intensity are reported with their standard deviation.

Grain size		Raman intensity values ± SD obtained for 3 replicates on binary mixtures			Mean ± SD
		(1)	(2)	(3)	
10 – 50 (µm)	I_{Gyp}	7400 ± 1100	7400 ± 1100	7100 ± 1000	7300 ± 200
	I_{Cys}	830 ± 200	820 ± 200	800 ± 200	820 ± 20
50 – 100 (µm)	I_{Gyp}	6800 ± 1300	6500 ± 1300	6700 ± 1300	6700 ± 200
	I_{Cys}	830 ± 200	790 ± 200	820 ± 200	810 ± 20
100 – 150 (µm)	I_{Gyp}	5900 ± 1400	5200 ± 1300	5200 ± 1200	5400 ± 400
	I_{Cys}	700 ± 100	600 ± 100	600 ± 200	660 ± 50

In order to compare Raman signal intensities in different studies, it is important to understand the factors that determine the Raman intensity. The Raman signal magnitude is generally addressed in two parts: one aspect is linked to the scattering intensity and the other linked to the collection and detection of scattered light.[23,24,44] The variables determining the scattering intensity include the laser irradiance (or power density), the Raman cross-section of the analyte and the sampled volume (related to the number of scatterers interrogated during the experiment). The collection optics and spectrograph also influence the Raman intensity by determining the fraction of the scattered light detected by the detector. The main parameters for describing the light collection optic efficiency are the NA and the f-number (f/#).

The irradiance, or laser power per surface unit (expressed in W/m^2 or W/cm^2) is a critical parameter for the Raman scattering intensity. Increasing the laser irradiance generally increases the Raman signal strength, up to a limit of sample radiation damage. Furthermore, the irradiance is directly related to the laser spot size on the sample.[36] For a given laser power, a smaller laser spot size leads to a higher irradiance, and vice-versa. Therefore, the effective laser spot size, defined here as the diameter of the laser footprint on the sample from which a Raman signal is detected with a given instrument, is an operating parameter that should be reported alongside with the laser power delivered on the sample when publishing Raman studies. This is especially important in the field of astrobiology where, in preparation for the future exploration missions of Mars, analog biogeological samples are thoroughly interrogated using various Raman instruments, from benchtop instruments (often offering a high spatial resolution, i.e., small spot size) to portable instruments (closer to miniaturized spectrometer for planetary exploration, but offering a lower spatial resolution, i.e., large spot size). In many published works, it is quite common to reference the laser power (most commonly the laser output power and not the laser power on the sample) at which the data were acquired. However, the laser power alone does not allow a comparison of the data obtained for similar samples with different instruments.

The knife-edge technique offers a straightforward method to determine the effective laser spot size across various Raman instruments, whether portable or benchtop microspectrometers. While the fitting procedure described here provides the beam radius at 1/e of its maximum intensity (ω), we recommend expressing the spot size as the beam diameter at $1/e^2$ (~13.5%) of maximum intensity (2ω'). Indeed, for Raman applications, a molecule at 2ω' from the beam center (thus receiving only 13.5% of the incident laser intensity received by another molecule at the center of the laser spot) can still contribute to the Raman spectrum, especially if the Raman cross-section of that molecule is high, such as resonant molecules (e.g., carotenoids).

The ability to determine the laser spot size of a given instrument is important for addressing specific research applications, especially when different focusing and collection optical accessories can be mounted on the Raman system. This consideration becomes particularly critical in the context of planetary exploration and astrobiology, where the laser spot size directly influences how effectively Raman spectroscopy can target and detect organic signatures embedded within mineral matrices during the investigation of biogeological samples. A small spot size provides a high spatial resolution and enables probing very specific micrometric areas on samples, with high irradiance, facilitating intense signal collection. Assuming no laser-induced thermal sample degradation, this Raman sampling is advantageous for characterizing planetary analogue samples, often presenting microdomains where biomarkers or carbonaceous matter (e.g., microbial patches or laminations) can be observed on top of (or included in) a bulk rock.

Conversely, a larger spot size provides a lower spatial resolution by illuminating the sample over larger surface areas, potentially encompassing both the organic targets and surrounding mineral matrix. In cases where the organic microdomain

is smaller than the laser spot, this dilution effect and reduced irradiance on the sample could significantly weaken the Raman signal of the organic analytes and compromise their detectability. However, for solid dispersions where the analyte is homogeneously dispersed in powdered rocks at low concentration, performing Raman measurements using a larger laser footprint is more advantageous than with a smaller laser spot. Even though a larger spot size results in lower irradiance (comparing instruments with identical laser power), the increased number of excited scatterers contributes to a higher Raman signal gain. This gain is even more important because the scattered light comes from the volume of the sample (effective sampling volume), not just its surface area (spot size). The sampling volume varies with the sample properties (e.g., clear or optically dense materials) and spectrometer properties, such as the depth of focus.[23] Thus, optimizing the Raman detectability involves a trade-off between several instrumental parameters, which must be tailored to the structural (i.e., bulk or powder rocks) and compositional characteristics (e.g., transparent or absorbing materials) of the sample under investigation. In optically clear materials such as gypsum, Raman spectrometers with low NAs and large spot sizes can probe depths of several hundred micrometers to a few millimeters, enhancing the likelihood of detecting analytes within the volume. An example of quantitative performances attainable for the Advantage 532 spectrometer applied on various mineral powder dispersions relevant to Mars spiked with organics can be found in Demaret et al.[39]

Finally, we demonstrated experimentally that the grainy structure of a powdered sample can significantly increase the effective spot size: 2ω' was approximately two times larger with gypsum grains (particle sizes ranging between 10 and 150 µm) than the effective spot size measured on the silicon wafer. The result is of most importance since the ExoMars sample preparation and delivery system (SPDS) will crush selected geological samples on Mars before interrogating them with the Raman laser spectrometer. When reporting the Raman detection of bio- and geomarkers in the scope of planetary missions, we therefore recommend to report data obtained for both crushed and uncrushed samples.

In the present study, we observed that both the effective laser footprint and the detected Raman intensity tend to increase as the average size of the grains decreases. This trend is likely due to enhanced diffuse reflectance, which allows the laser beam to interact with a greater number of Raman-active molecules.[45] However, this observation contrasts with theoretical predictions based on the Kubelka–Munk model and some experimental studies, which suggest that Raman intensity should increase with increasing grain size.[46,47] This discrepancy appears to be strongly influenced by the optical configuration of the Raman systems, particularly the illumination and collection geometry. Specifically, a decrease in Raman intensity is typically observed for dispersions with smaller grain sizes when using micro-Raman systems with small laser footprints (e.g.,<5 µm).[48–50] In contrast, instruments with larger laser footprints (e.g.,>100 µm) often lead to increased Raman intensity as the grain size decreases.[45,51] Recent studies have shown that both trends can coexist within a single system when a broad range of grain sizes is tested using portable or handheld Raman instruments.[52–55] In these cases, Raman intensity typically increases with decreasing grain size up to a certain point, after which it declines again. This suggests that intermediate grain sizes may offer optimal measurement conditions, likely due to improved packing density (i.e., reduced porosity) and minimized surface effects such as grain boundary scattering or surface defects. While our datasets include a limited range of grain size fractions, preventing a full assessment of the influence of particle packing or surface characteristics on the Raman signal intensity, our results nonetheless indicate that light collection efficiency plays a critical role. As the laser spot enlarges due to the grain size effect, the collection optics of our Raman system are able to gather more scattered photons, resulting in a net increase in Raman intensity. Future studies using miniaturized Raman systems and various (organo-)mineral dispersions are needed to further elucidate the relationship between analytical performance, detection limits, and grain size effects, particularly in the context of planetary exploration missions. This includes upcoming deployments such as the ExoMars 2028 mission, where the RLS instrument will analyze crushed core sample material.

Conclusion

The knife-edge technique, which is an experimental scanning measurement method for evaluating the laser beam radii (hence the laser beam diameter), was successfully employed with various Raman spectrometers. The knife-edge technique offers a fast, non-expensive, and practical tool for documenting the effective spot size of Raman systems, especially when granular solid materials are analyzed. The effective experimental laser footprint of various instruments was determined on solid samples, either a flat silicon wafer or granular gypsum dispersions. We emphasize that interrogating gypsum powders led to an important enlargement (a twofold increase) of the laser footprint comparatively to the laser footprint evaluated on the silicon wafer. We also discussed that characterizing the effective spot size can have important implications for the outcomes of Raman analyses, either qualitative (ability to discriminate between close particles, i.e., Raman spatial resolution) or quantitative (number of scattered Raman photons collected, i.e., Raman intensity), as indicated by the variation of Raman

intensity observed with the grain size of various gypsum powders. Measuring the effective focal spot size can have a significant impact for comparing Raman data obtained with various instruments, for instance in the context of planetary exploration where various powdered rocks and soils are analyzed by Raman spectroscopy.

Acknowledgments

The authors are grateful to Raymond Vanderlinden for kindly providing mineral samples (private collection) for this study.

Declaration of Conflicting Interests

The authors declared no potential conflicts of interest with respect to the research, authorship, and/or publication of this article.

Funding

The authors disclosed receipt of the following financial support for the research, authorship, and/or publication of this article: This work was supported by the F.R.S.-FNRS (Grant nos. FNRS32763312 and FNRS-29327850) and the UK Space Agency (Grant nos. ST/T007281/1, ST/T00729X/1, and ST/V006290/1).

References

1. P. Vitek, E.M.A. Ali, H.G.M. Edwards, J. Jehlička, et al. “Evaluation of Portable Raman Spectrometer with 1064 nm Excitation for Geological and Forensic Applications”. Spectrochim. Acta, Part A. 2012. 86: 320–327. 10.1016/j.saa.2011.10.043
2. P. Vandenabeele, H.G.M. Edwards, J. Jehlička. “The Role of Mobile Instrumentation in Novel Applications of Raman Spectroscopy: Archaeometry, Geosciences, and Forensics”. Chem. Soc. Rev. 2014. 43(8): 2628–2649. 10.1039/c3cs60263j
3. K. Kong, C. Kendall, N. Stone, I. Notingher. “Raman Spectroscopy for Medical Diagnostics: From In-Vitro Biofluid Assays to In-Vivo Cancer Detection”. Adv. Drug Deliv. Rev. 2015. 89: 121–134. 10.1016/j.addr.2015.03.009
4. J. Jehlička, A. Culka. “Critical Evaluation of Portable Raman Spectrometers: From Rock Outcrops and Planetary Analogs to Cultural Heritage: A Review”. Anal. Chim. Acta. 2022. 1209: 339027. 10.1016/j.aca.2021.339027
5. J.L. Vago, F. Westall, A.J. Coates, R. Jaumann, et al. “Habitability on Early Mars and the Search for Biosignatures with the ExoMars Rover”. Astrobiology. 2017. 17(6–7): 471–510. 10. 1089/ast.2016.1533
6. F. Rull, S. Maurice, I. Hutchinson, A. Moral, et al. “The Raman Laser Spectrometer for the ExoMars Rover Mission to Mars”. Astrobiology. 2017. 17(6–7): 627–654. 10.1089/ast.2016.1567
7. R. Bhartia, R.W.Beegle, L.Deflores, W.Abbey, et al. “Perseverance’s Scanning Habitable Environments with Raman and Luminescence for Organics and Chemicals (SHERLOC) Investigation”. Sci. Space Rev. 2021. 217: 58. 10.1007/s11214-021-00812-z
8. H.G.M. Edwards, S.E.J. Villar, J. Jehlička, T. Munshi. “FT-Raman Spectroscopic Study of Calcium-Rich and Magnesium-Rich Carbonate Minerals”. Spectrochim. Acta, Part A. 2005. 61 (10): 2273–2280. 10.1016/j.saa.2005.02.026
9. S.E. Jorge-Villar, H.G.M. Edwards. “Raman Spectroscopy in Astrobiology”. Anal. Bioanal. Chem. 2006. 384(1): 100–113. 10.1007/s00216-005-0029-2
10. A. Wang, R.L. Korotev, B.L. Jolliff, Z. Ling. “Raman Imaging of Extraterrestrial Materials”. Planet. Space Sci. 2015. 112: 23– 34. 10.1016/j.pss.2014.10.005
11. J.M. Stromberg, A. Parkinson, M. Morison, E. Cloutis, et al. “Biosignature Detection by Mars Rover Equivalent Instruments in Samples from the CanMars Mars Sample Return Analogue Deployment”. Planet. Space Sci. 2019. 176: 104683. 10.1016/j. pss.2019.06.007
12. F. Rull, M. Veneranda, J.A. Manrique-Martinez, A. Sanz-Arranz, et al. “Spectroscopic Study of Terrestrial Analogues to Support Rover Missions to Mars: A Raman-Centred Review”. Anal. Chim. Acta. 2022. 1209: 339003. 10.1016/j.aca.2021. 339003
13. L. Demaret, I.B. Hutchinson, R. Ingley, H.G.M. Edwards, et al. “Fe-Rich Fossil Vents as Mars Analog Samples: Identification of Extinct Chimneys in Miocene Marine Sediments Using Raman Spectroscopy, X-ray Diffraction, and Scanning Electron Microscopy–Energy Dispersive X-ray Spectroscopy”. Astrobiology. 2022. 22(9): 1081–1098. 10.1089/ast.2021.0128
14. H.G.M. Edwards, P. Vandenabeele, S.E. Jorge-Villar, E.A. Carter, et al. “The Rio Tinto Mars Analogue Site: An Extremophilic Raman Spectroscopic Study”. Spectrochim. Acta, Part A. 2007. 68(4): 1133–1137. 10.1016/j.saa.2006.12.080
15. U. Böttger, J.-P. de Vera, J. Fritz, I. Weber, et al. “Optimizing the Detection of Carotene in Cyanobacteria in a Martian Regolith Analogue with a Raman Spectrometer for the ExoMars Mission”. Planet. Space Sci. 2012. 60(1): 356–362. 10.1016/j. pss.2011.10.017
16. P. Vitek, J. Jehlička, H.G.M. Edwards, I. Hutchinson, et al. “The Miniaturized Raman System and Detection of Traces of Life in Halite from the Atacama Desert: Some Considerations for the Search for Life Signatures on Mars”. Astrobiology. 2012. 12(12): 1095–1099. 10.1089/ast.2012.0879
17. H.G.M. Edwards, I.B. Hutchinson, R. Ingley, J. Parnell, et al. “Raman Spectroscopic Analysis of Geological and Biogeological Specimens of Relevance to the ExoMars Mission”. Astrobiology. 2013. 13(6): 543–549. 10.1089/ast.2012.0872

18. J.Jehlička,A. Oren. “RamanSpectroscopyin Halophile Research”. Front. Microbiol. 2013. 4: 380. 10.3389/fmicb.2013.00380
19. J. Jehlička, H.G.M. Edwards, A. Oren. “Raman Spectroscopy of Microbial Pigments”. Appl. Environ. Microbiol. 2014. 80(11): 3286–3295. 10.1128/AEM.00699-14
20. C. Malherbe, R. Ingley, I. Hutchinson, H. Edwards, et al. “Biogeological Analysis of Desert Varnish Using Portable Raman Spectrometers”. Astrobiology. 2015. 15(6): 442–452. 10.1089/ast.2014.1265
21. C.P. Marshall, A. Olcott Marshall. “Challenges Analyzing Gypsum on Mars by Raman Spectroscopy”. Astrobiology. 2015. 15(9): 761–769. 10.1089/ast.2015.1334
22. P. Vandenabeele, J. Jehlička, P. Vitek, H.G.M. Edwards. “On the Definition of Raman Spectroscopic Detection Limits for the Analysis of Biomarkers in Solid Matrices”. Planet. Space Sci. 2012. 62(1): 48–54. 10.1016/j.pss.2011.12.006
23. R.L. McCreery. Raman Spectroscopy for Chemical Analysis. New York: John Wiley and Sons, 2000.
24. G. Turrell, J. Corset. Raman Microscopy: Developments and Applications. London: Academic Press, 1996.
25. J.A. Ruff, A.E. Siegman. “Single-Pulse Laser Beam Quality Measurements Using a CCD Camera System”. Appl. Opt. 1992. 31(24): 4907–4909. 10.1364/AO.31.004907
26. R.L. McCally. “Measurement of Gaussian Beam Parameters”. Appl. Opt. 1984. 23(14): 2227. 10.1364/ao.23.002227
27. D. Letalick, I. Renhorn. “Instrument for Measuring Laser-Beam Profiles”. Rev. Sci. Instrum. 1987. 58(5): 765–767. 10.1063/1. 1139628
28. K.C. Jorge, R. Riva, N.A.S. Rodrigues, J.M.S. Sakamoto, M.G. Destro. “Scattered Light Imaging Method (SLIM) for Characterization of Arbitrary Laser Beam Intensity Profiles”. Appl. Opt. 2014. 53(20): 4555–4564. 10.1364/AO.53.004555
29. P.J. Shayler. “Laser Beam Distribution in the Focal Region”. Appl. Opt. 1978. 17(17): 2673–2684. 10.1364/AO.17.002673
30. J.M. Liu. “Simple Technique for Measurements of Pulsed Gaussian-Beam Spot Sizes”. Opt. Lett. 1982. 7(5): 196–198. 10.1364/OL.7.000196
31. J.M. Khosrofian, B.A. Garetz. “Measurement of a Gaussian Laser Beam Diameter Through the Direct Inversion of Knife-Edge Data”. Appl. Opt. 1983. 22(21): 3406–3410. 10.1364/AO.22. 003406
32. Z.A. Talib, W.M.M. Yunus. “Measuring Gaussian Laser Beam Diameter Using Piezoelectric Detection”. Meas. Sci. Technol. 1993. 4(1): 22–25. 10.1088/0957-0233/4/1/004
33. Y. Chiu, J.-H. Pan. “Micro Knife-Edge Optical Measurement Device in a Silicon-on-Insulator Substrate”. Opt. Express. 2007. 15(10): 6367–6373. 10.1364/OE.15.006367
34. M.A.C. de Araújo, R. Silva, E. de Lima, D.P. Pereira, P.C. de Oliveira. “Measurement of Gaussian Laser Beam Radius Using the Knife-Edge Technique: Improvement on Data Analysis”. Appl. Opt. 2009. 48(2): 393–396. 10.1364/AO.48.000393
35. P. Hauer, J. Grand, A. Djorovic, G. R. Willmott, E.C. Le Ru. “Spot Size Engineering in Microscope-Based Laser Spectroscopy”. J. Phys. Chem. C. 2016. 120(37): 21104– 21113. 10.1021/acs.jpcc.6b04574
36. F. Foucher. “Influence of Laser Shape on Thermal Increase During Micro-Raman Spectroscopy Analyses”. J. Raman Spectrosc. 2022. 53(3): 664–676. 10.1002/jrs.6230
37. I. de Wolf. “Semiconductors”. In: M.J. Pelletier, editor. Analytical Applications of Raman Spectroscopy. Malden, Massachusetts: Blackwell Science, 1999. Chap. 10, Pp. 435–472.
38. L. Demaret, I.B. Hutchinson, G. Eppe, C. Malherbe. “Analytical Strategy for Representative Subsampling of Raman-Based Robotic Planetary Exploration Missions: The Case Study of Solid Dispersions of β-Carotene and L-Cysteine in Gypsum”. J. Raman Spectrosc. 2020. 51(9): 1624–1635. 10.1002/jrs.5705
39. L. Demaret, I.B. Hutchinson, G. Eppe, C. Malherbe. “Quantitative Analysis of Binary and Ternary Organo-Mineral Solid Dispersions by Raman Spectroscopy for Robotic Planetary Exploration Missions on Mars”. Analyst. 2021. 146 (23): 7306–7319. 10.1039/D1AN01514A
40. H. Kogelnik, T. Li “Laser Beams and Resonators“. Appl. Opt. 1966. 5(10): 1550–1567. 10.1364/AO.5.001550
41. W. Demtröder. “Optics of Gaussian Beams”. Laser Spectroscopy 1: Basic Principles. Berlin; Heidelberg: Springer, 2014. Pp. 421–429. 10.1007/978-3-642-53859-9_7
42. I.B. Hutchinson, R. Ingley, H.G.M. Edwards, L. Harris, et al. “Raman Spectroscopy on Mars: Identification of Geological and Bio-Geological Signatures in Martian Analogues Using Miniaturized Raman Spectrometers”. Philos. Trans. R. Soc., A. 2014. 372(2030): 20140204. 10.1098/rsta.2014.0204
43. L.A. Haskin, A. Wang, K.M. Rockow, B.L. Jolliff, et al. “Raman Spectroscopy for Mineral Identification and Quantification for In Situ Planetary Surface Analysis: A Point Count Method”. J. Geophys. Res.: Planets. 1997. 102(E8): 19293–19306. 10. 1029/97JE01694
44. M.J. Pelletier. “Raman Instrumentation”. In: M.J. Pelletier, editor. Analytical Applications of Raman Spectroscopy. Malden, Massachusetts: Blackwell Science, 1999. Chap. 2, Pp. 53–105.
45. H. Wang, C.K. Mann, T.J. Vickers.“Effect of Powder Properties on the Intensity of Raman Scattering by Crystalline Solids”. Appl. Spectrosc. 2002. 56(12): 1538–1544. 10.1366/000370202321115779
46. B. Schrader, A. Hoffman, S. Keller. “Near-Infrared Fourier Transform Raman Spectroscopy: Facing Absorption and Background”. Spectrochim. Acta, Part A. 1991. 47(9–10): 1135–1148. 10.1016/ 0584-8539(91)80201-S

47. P.K. Duy, S. Chun, H. Chung. “Characterization of Raman Scattering in Solid Samples with Different Particle Sizes and Elucidation on the Trends of Particle Size-Dependent Intensity Variations in Relation to Changes in the Sizes of Laser Illumination and Detection Area”. Anal. Chem. 2017. 89(22): 11937–11943. 10.1021/acs.analchem.7b01400
48. A. Wang. “Some Grain Size Effects on Raman Scattering Intensity for In Situ Measurements on Rocks and Soils Experimental Tests and Modeling”. 30th Annual Lunar Planetary Science Conference. Houston, Texas; 15–20 March 1999. Abstract no. 1644. https://www.lpi.usra.edu/meetings/ LPSC99/pdf/1644.pdf [accessed 19 November 2025].
49. C.H. Chio, S.K. Sharma, P.G. Lucey, D.W. Muenow. “Effects of Particle Size and Laser-Induced Heating on the Raman Spectra of Alpha Quartz Grains”. Appl. Spectrosc. 2003. 57(7): 774– 783. 10.1366/000370203322102852
50. F. Foucher, G. Lopez-Reyes, N. Bost, F. Rull-Perez, et al. “Effect of Grain Size Distribution on Raman Analyses and the Consequences for In Situ Planetary Missions”. J. Raman Spectrosc. 2013. 44: 916–925. 10.1002/jrs.4307
51. M.V. Pellow-Jarman, P.J. Hendra, R.J. Lehnert. “The Dependence of Raman Signal Intensity on Particle Size for Crystal Powders”. Vib. Spectrosc. 1996. 12(2): 257–261. 10.1016/0924-2031(96) 00023-9
52. P. Kristova, L.J. Hopkinson, K.J. Rutt, H. Hunter, G. Cressey. “Quantitative Analyses of Powdered Multi-Minerallic Carbonate Aggregates Using a Portable Raman Spectrometer”. Am. Mineral. 2013. 98(2–3): 401–409. 10. 2138/am.2013.4305
53. P. Kristova, L.J. Hopkinson, K.J. Rutt. “The Effect of the Particle Size on the Fundamental Vibrations of the [$CO^2{}_3{}^-$] Anion in Calcite”. J. Phys. Chem. A. 2015. 119: 4891–4897. 10.1021/ acs.jpca.5b02942
54. C. Indelicato, I. Osticioli, J. Agresti, D. Ciofini, et al. “Exploring Grain Sizing of Sedimentary Calcareous Rocks Using Raman Spectroscopy”. Eur. Phys. J. Plus. 2022. 137: 359. 10.1140/ epjp/s13360-022-02536-7
55. L.B. Breitenfeld, M.D. Dyar, E.C. Sklute, C. Legett. “Effect of Particle Size on Raman Signal Strength of Silicate Minerals”. J. Raman Spectrosc. 2025. 56(2): 184–187. 10. 1002/jrs.6745